catalysts

MDPI

Article

TiO_2 and TiO_2-Carbon Hybrid Photocatalysts for Diuron Removal from Water

Ana Amorós-Pérez [1], María Ángeles Lillo-Ródenas [1,*], María del Carmen Román-Martínez [1], Patricia García-Muñoz [2] and Nicolas Keller [2]

[1] Materiales Carbonosos y Medio Ambiente (MCMA) Group, Department of Inorganic Chemistry and Materials Institute (IUMA), Faculty of Sciences, University of Alicante, Ap. 99, E-03080 Alicante, Spain; ana.amoros@ua.es (A.A.-P.); mcroman@ua.es (M.d.C.R.-M.)

[2] Institut de Chimie et Procédés pour l'Energie, l'Environnement et la Santé, Centre National de la Recherche Scientifique (CNRS) et Université d'Strasbourg, 25 rue Becquerel, 67087 Strasbourg, France; patricia.gmunoz@upm.es (P.G.-M.); nkeller@unistra.fr (N.K.)

* Correspondence: mlillo@ua.es; Tel.: +34-965-903-545; Fax: +34-965-903-454

Abstract: TiO_2 and TiO_2-activated carbon (AC) photocatalysts have been prepared (by sol-gel synthesis), characterized, and tested in the removal of diuron from water under simulated solar light. The preparation variables of the two series of catalysts are: (i) heat-treatment temperature of bare TiO_2 (350, 400, 450 and 500 °C) and (ii) activated carbon content (0.5, 1, 5, and 10 wt.%) in TiO_2-AC samples heat-treated at 350 °C. The activated carbon was previously prepared by hydrothermal carbonization of saccharose and has spherical shape. The heat-treatment temperature does not determine the efficiency of TiO_2 for diuron photocatalytic degradation but clearly influences the diuron adsorption capacity. The capacity of TiO_2-AC samples for diuron removal increases with the carbon content and it is the result of combined diuron adsorption and photodegradation. Thus, the sample with highest carbon content (10 wt.% nominal) leads to the highest diuron removal. The TiO_2-AC photocatalysts have proved to be capable of degrading diuron previously adsorbed in dark conditions, which allows their regeneration.

Keywords: photocatalysis; TiO_2; activated carbon; diuron; solar chamber

Citation: Amorós-Pérez, A.; Lillo-Ródenas, M.Á.; Román-Martínez, M.d.C.; García-Muñoz, P.; Keller, N. TiO_2 and TiO_2-Carbon Hybrid Photocatalysts for Diuron Removal from Water. *Catalysts* **2021**, *11*, 457. https://doi.org/10.3390/catal11040457

Academic Editor: Simonetta Palmas

Received: 24 February 2021
Accepted: 30 March 2021
Published: 1 April 2021

1. Introduction

As intensive agriculture involves the use of large quantities of herbicides, they are becoming emerging pollutants whose concentration in waters and soils is alarmingly increasing all over the world. Herbicides are toxic and usually persistent compounds, being thus very harmful for natural ecosystems [1]. Moreover, the problem of available water resources scarcity is growing in many areas of the Earth. Hence, the development of efficient and cheap methods to treat aqueous effluents is a scientific and technical challenge. Although biodegradation of organic/inorganic pollutants is often viable, a variety of pollutants, such as some pesticides, are recalcitrant to conventional biological treatments [2]. For this reason, more powerful degradation technologies are required.

Diuron (3-(3,4-dichlorophenyl)-1,1-dimethylurea) is one of the most commonly used herbicides [3], employed to control a wide variety of weeds and mosses, to protect many agricultural crops and to keep clean non-crop areas [4]. Dispersion of this compound leads to aquatic environments pollution by soil leaching [5,6], and it appears to be moderately persistent in water [7]. Diuron has been reported to be present in 70% of the rivers in 27 European countries, with concentration peaks up to 0.826 μg/L [8]. It is considered a real environmental hazard, demonstrated in 2013 by an issued law of the European Commission that included diuron in the list of priority pollutants in water treatment policy [9].

Advanced oxidation processes such as heterogeneous photocatalysis is one of the promising techniques for the abatement of water pollutants [1,10–14]. Photocatalysis can

be considered advantageous over existing disinfection methods, such as chlorination or ozonation, because the process is self-sustaining and the regular replenishment of treatment products can be avoided [1]. Titanium dioxide is one of the most used photocatalysts due to properties such as good efficiency, low cost, nontoxicity, and stability. Anatase is usually regarded as the most photoactive TiO_2 phase, mainly because of the lower e^-/h^+ pairs recombination rate and the 3.20 eV wide band-gap [15–17]. Solar photocatalysis on TiO_2 has proved to allow total detoxification of aqueous diuron solutions in parallel to a complete mineralization of the pollutant [18,19]. However, it is still necessary to increase its photoactivity and efficiency.

As the photocatalytic activity of TiO_2 depends on physicochemical properties such as surface area, surface chemistry, crystallinity degree, phase composition, and crystal size, it is expected that an appropriate combination of these parameters would lead to very efficient photocatalysts [17,20–22]. The mentioned properties can be modified, in a certain range, varying the preparation conditions. Moreover, the incorporation of other chemical elements or compounds has been also considered to be a way to improve the TiO_2 photocatalytic efficiency. Visible-light-induced photoreactivity of TiO_2 was improved by doping with metals [23–26], coupling with other semiconductors [24,27] or adding non-metal component(s), such as carbon. Carbonaceous materials have attracted attention as additives or components to prepare hybrid TiO_2-C photocatalysts, mainly because of their unique and controllable structural and electrical properties [21,28,29]. The review work of Leary and Atwood [28] highlights the progress and development of nanocarbon-TiO_2 photocatalysts and states that they have the potential to address the three aspects that may bring an enhancement of the photocatalytic activity: (i) band-gap tuning or extension of excitation wavelength through photosensitization, (ii) retardation of electron–hole recombination, and (iii) provision of high-surface area for adsorption of reactants and of active sites.

The Ngo's group has investigated the photocatalytic degradation of metsulfuron-methyl herbicide using TiO_2 and a small amount of powdered activated carbon (AC) as catalyst. These authors reported that hybrid TiO_2-AC samples lead to significant better performance in herbicide removal than the independent adsorption by AC or the photocatalytic degradation by TiO_2 [30,31]. Bamba et al. studied the activity of TiO_2 prepared by sol-gel deposited on carbon materials such as AC, graphite, and carbon aerogel, for diuron photodegradation [32]. They found that TiO_2/AC and TiO_2/carbon aerogel samples were promising under sunlight irradiation, attributing the good behavior to a high anatase crystallinity, high specific surface area, and large pore volume.

The photocatalysts' regeneration efficiency is also another important property from the point of view of the practical applicability of the prepared photocatalysts. A few studies have been carried out on the recyclability of photocatalysts used in diuron degradation. For example, Anirudhan et al. proved that photocatalysts like, ZnO nanorod decorated carboxylic graphene/polyaniline composite photocatalysts [33] and TiO_2-based ones [34] can be used and regenerated at least for five cycles. However, no studies have been found to date to prove the recyclability of TiO_2-AC materials as photocatalysts for diuron degradation.

In general, the photoactivity of the carbon-TiO_2 hybrid photocatalysts depends on the carbon content but also, as in the case of pure TiO_2, on physicochemical parameters such as crystal structure, crystallite size and surface area [35,36] which, in turn, depend, among others, on the temperature of the post-synthesis crystallization heat treatment [37].

Considering the presented ideas, this work addresses the preparation by sol-gel of two series of samples: pure TiO_2 samples submitted to a post-synthesis heat treatment at a temperature ranging from 350 to 500 °C; and TiO_2-AC hybrid samples containing different amounts of a spherical activated carbon for which the post-synthesis heat-treatment temperature was 350 °C, and the study of their use for the removal of diuron from water under simulated solar light, including regeneration efficiency. In fact, comparison between these

two series, prepared in the same conditions, lets us analyze the importance of the carbon presence. Their regeneration has also been studied.

2. Results and Discussion

2.1. Determination of the Carbon Content in TiO_2-AC Samples

The thermogravimetry (TG) curves of the TiO_2-ACx (350) series (x = 0, 0.5, 1, 5, and 10) (Figure S1a in Supplementary Materials) show three small weight losses at, approximately, 80, 180 and 330 °C, and a main weight loss from 450 to 650 °C. Differential thermogravimetry (DTG) profiles (Figure S1b in Supplementary Materials) have allowed to precisely locate the temperature of the weight losses. The first two weight losses are due, respectively, to adsorbed water and organic residues remaining from the TiO_2 synthesis [38,39]. The third one is only evident in the TiO_2-AC10 (350) sample, and corresponds to the decomposition of surface oxygen groups of the activated carbon [40]. The largest weight loss is due to combustion of carbon and the removal of oxygen-containing groups [41]. The weight loss related to the phase transformation from amorphous TiO_2 to anatase can also occur in the 450 to 650 °C range [42], but it is small compared to that due to the carbon combustion. Such a weight loss has been quantified for sample TiO_2 (350) in a similar TG experiment and it amounts about 0.2%.

Thus, the carbon content of the TiO_2-ACx (350) samples has been calculated by subtracting the weight loss corresponding to the transformation of amorphous TiO_2 to anatase from the weight loss observed between 450 and 650 °C. The calculated carbon content was: 0.0, 0.4, 0.5, 3.6 and 8.3 wt.% for TiO_2-ACx (350) samples (x = 0, 0.5, 1, 5, and 10, respectively). The complete quantification of the TG profiles can be seen in Table S1 (Supplementary Materials).

2.2. Textural Properties

Figure 1a shows the N_2 adsorption-desorption isotherms of TiO_2 (nt), TiO_2 (T) and P25 samples. All the photocatalysts showed an isotherm type IV according to the IUPAC (International Union of Pure and Applied Chemistry) classification [43], with a hysteresis loop typical of the presence of mesoporosity. The hysteresis loop in the isotherms of the TiO_2 (nt) and TiO_2 (T) samples is type H2 [43], indicating the presence of cylindrical pores with narrow and wide necks, and a certain contribution of "ink bottle" or bottle-type pores [44], while it is type H3 in the isotherm of P25, usually given by non-rigid aggregates of plate-like particles forming slit-like pores [44]. The calculated values of surface area and pore volume are collected in Table S2 (Supplementary Materials) showing that most of them are higher for the prepared samples than for P25 and decrease as the temperature of the heat treatment increases (Brunauer–Emmett–Teller (BET) surface area from 296 to 45 m^2/g, mesopore volume from 0.17 to 0.07 cm^3/g and total pore volume decrease from 0.32 to 0.09 cm^3/g). In the literature this is usually explained as a consequence of the crystallite size growth upon heating [45,46]. The prepared TiO_2 materials have surface areas in the same order of magnitude, or even larger, than those of other materials prepared in similar conditions [46,47].

Figure 1b shows the N_2 adsorption-desorption isotherms of the prepared AC and of the TiO_2 (350) and TiO_2-ACx (350) samples, while the calculated surface area and pore volume are included in Table S2. The N_2 adsorption-desorption isotherms of AC is type I, characteristic of an essentially microporous solid [43], for which the S_{BET} is 491 m^2/g, and those of the TiO_2-ACx (350) samples are type IV with H2-type hysteresis loops, revealing that these samples are mesoporous. All of them show a rather similar adsorption capacity, slightly higher than that of the bare TiO_2 samples (from 144 for TiO_2 (350) up to 173 m^2/g for the TiO_2-AC10 (350) sample). The surface area of the TiO_2-ACx samples is the expected one according to the proportion of TiO_2 and AC.

The pore size distributions of the photocatalysts are compiled in Figure S2. They are very similar for all the prepared samples, showing a monomodal distribution ranging

between 3 and 18 nm (mainly based on mesopores), and with a mean pore diameter similar for most samples, around 8–9 nm, except for TiO_2 (nt).

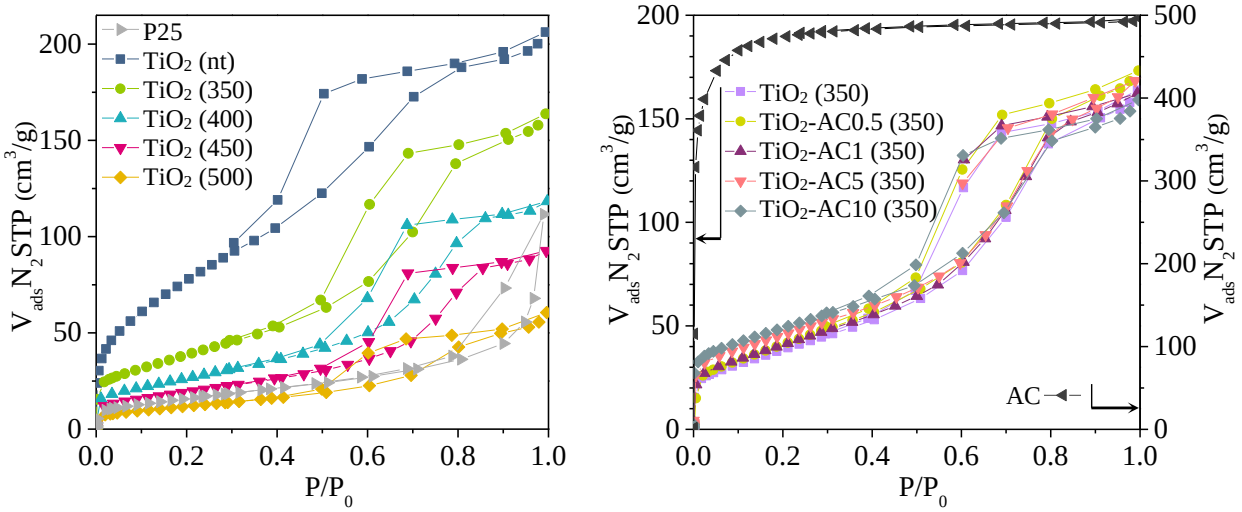

Figure 1. N_2 adsorption-desorption isotherms at −196 °C for: (**a**) P25, TiO_2 (nt) and TiO_2 (T) samples and (**b**) AC, TiO_2 (350) and TiO_2-ACx (350) samples.

2.3. X-ray diffraction (XRD) Analysis

The XRD patterns of P25, TiO_2 (nt), TiO_2 (T) and TiO_2-ACx (350) samples (Figure 2) show that P25 contains anatase and rutile, while the prepared photocatalysts contain only anatase [48,49].

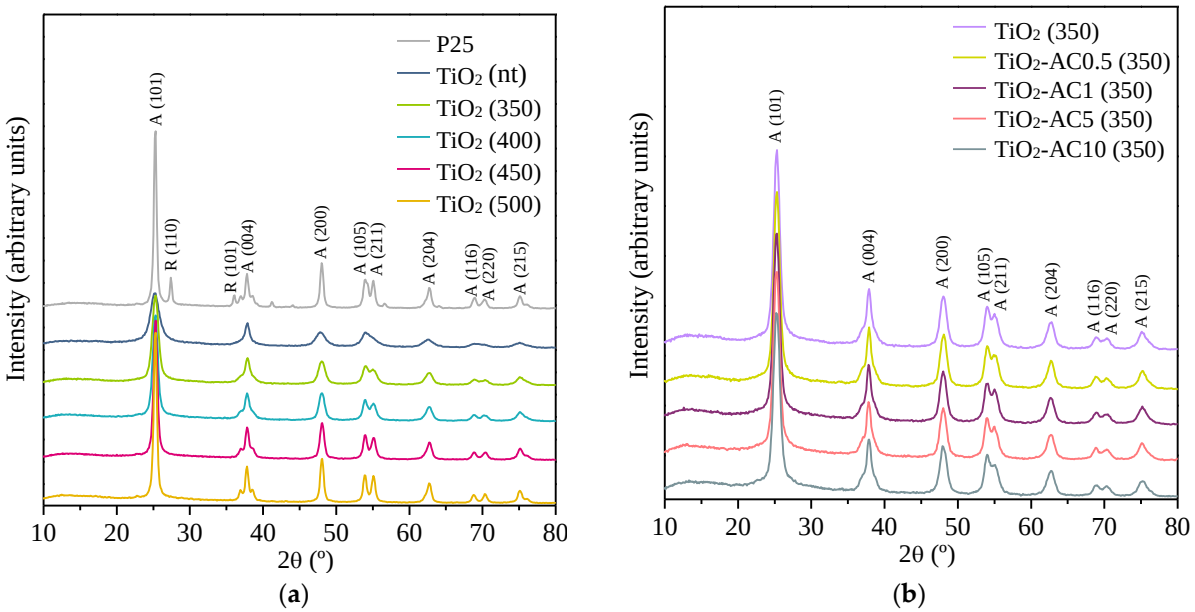

Figure 2. XRD patterns for: (**a**) P25, TiO_2 (nt) and TiO_2 (T) samples, and (**b**) AC, TiO_2-ACx (350) (x = 0, 0.5, 1, 5, and 10 wt.%) samples. The 2θ values of the TiO_2 characteristic diffraction peaks are: Anatase (A) (ref. JCPDS No. 21-1272): 25.3° (101), 37.8° (004), 48.0° (200), 54.5° (105), 55° (211), 62.7° (204), 70.4° (116) and 74.5° (220); and Rutile (R) (ref. JCPDS No. 21-1276): 27.5° (110), 36.1° (101) and 54.4° (211).

Quantification of crystalline phases and amorphous TiO_2 in each sample was performed following the procedure reported by Jensen et al. [50], which is described in detail in a previous publication [23]. The mean crystallite size has been calculated as indicated in the experimental section. Table 1 shows the obtained results.

Table 1. Crystalline and amorphous TiO_2 contents as well as mean crystallite size for P25, TiO_2 (nt) and TiO_2 (T) samples (Set 1) and for TiO_2-ACx (350) (x = 0, 0.5, 1, 5, and 10 wt.%) samples (Set 2).

Set	Sample	Crystalline Phase Amount (%)		Amorphous TiO_2 (%)	Average Crystallite Size (nm)	
		A	R		A	R
1	P25	73	14	13	22	28
	TiO_2 (nt)	62	-	38	6	-
	TiO_2 (350)	76	-	24	9	-
	TiO_2 (400)	76	-	24	10	-
	TiO_2 (450)	77	-	23	14	-
	TiO_2 (500)	78	-	22	16	-
2	TiO_2 (350)	76	-	24	9	-
	TiO_2-AC0.5 (350)	74	-	26	9	-
	TiO_2-AC1 (350)	74	-	26	8	-
	TiO_2-AC5 (350)	73	-	27	8	-
	TiO_2-AC10 (350)	74	-	26	8	-

A = Anatase, R = Rutile.

Data of Set 1 in Table 1 show that TiO_2 (nt) and TiO_2 (T) samples present high crystallinity, although they are less crystalline than P25, which is consistent with their surface areas since a lower surface area could be associated with: higher crystallinity and/or larger crystallite size (grain coarsening) or with some agglomeration. Even the not thermally treated sample (TiO_2 (nt)) shows high crystallinity (62%). It is important to mention that the anatase content of the TiO_2 (T) samples is similar, or even slightly higher, than that of P25. As expected, the increase of the heat-treatment temperature leads to an increase of the anatase content (from 62 to 78%) and of the anatase crystallite size (from 6 to 16 nm). This increase in crystalline size could be accompanied by a reduction in the BET surface area (Table S2) values.

Samples TiO_2-ACx (350) (Table 1, Set 2) contain, as well, only anatase. The anatase content and crystallite size is similar in TiO_2-ACx (350) samples and in TiO_2 (350), meaning that the incorporation of AC does not significantly influence the crystallinity of the synthesized TiO_2, independently of the AC wt.% content. The XRD pattern of the synthesized AC (reported in Supplementary Materials, Figure S3) corresponds to an amorphous material.

2.4. Scanning Electron Microscopy (SEM)

SEM images obtained for AC and for TiO_2-ACx samples before the heat treatment at 350 °C are shown in Figure 3. Figure 3a shows that the obtained AC presents spherical morphology (with 6.25 ± 1.02 μm average diameter size). TiO_2-ACx samples before the heat treatment are shown in Figure 3b–f. It is expected that this aspect does not significantly change after the heat treatment because it leads to very small loss of the carbon content. AC cannot be observed in the SEM images of the TiO_2-AC5 (nt) and TiO_2-AC1 (nt) samples, while it is clearly seen in the case of TiO_2-AC5 (nt) and TiO_2-AC10 (nt). It can be noted that TiO_2 particles are deposited on the AC spheres, and these two materials do not mix intimately (in agreement with the preserved TiO_2 crystallinity in the TiO_2-AC samples). By comparison of the images in Figure 3a,e,f it can be inferred that the carbon spheres are covered by a TiO_2 layer in TiO_2-ACx (nt) materials.

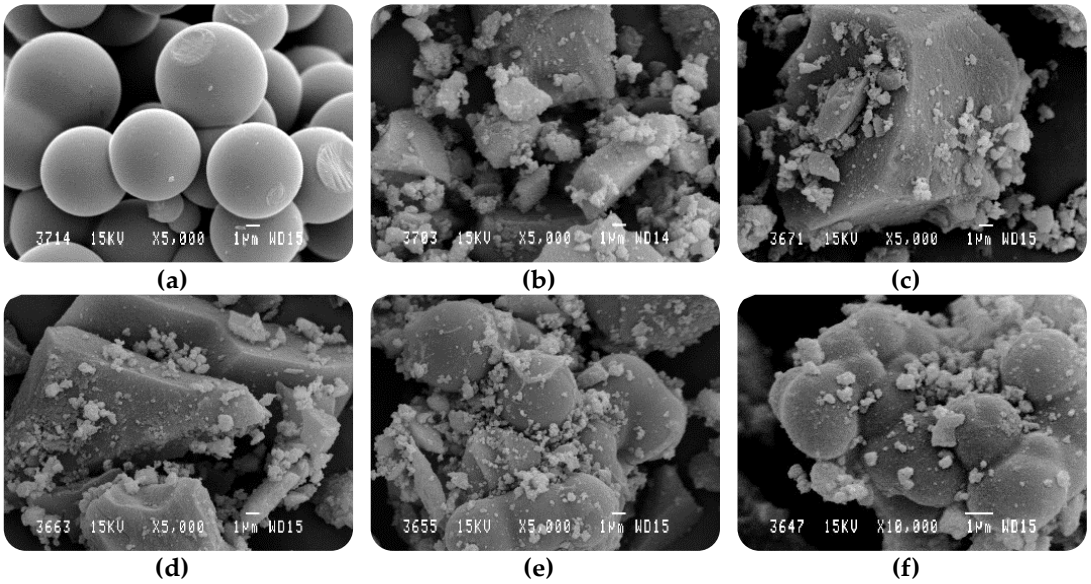

Figure 3. SEM images of: (**a**) AC, (**b**) TiO_2 (nt), (**c**) TiO_2-AC0.5 (nt), (**d**) TiO_2-AC1 (nt), (**e**) TiO_2-AC5 (nt) and (**f**) TiO_2-AC10 (nt).

2.5. Diuron Removal in Water

Figure 4 shows the plots of the relative diuron concentration C/C_s *versus* time (where C and C_s are, respectively, diuron concentration at a certain time t and the initial one, at t = −120 min) measured at certain time intervals under dark and illumination conditions. Figure 4a shows data obtained in experiments carried out using TiO_2 (nt), TiO_2 (T) samples and P25 and in a blank experiment carried out to evaluate diuron photolysis, if any, while Figure 4b shows the results obtained with TiO_2-ACx (350) sample, including TiO_2 (350) for comparison. The plots are divided in two zones: the first 120 min (negative numbers in *x*-axis) correspond to dark conditions and from the time identified as 0, the system is irradiated. Diuron concentration at t = 0 is identified as C_0. Plots of $Ln(C_0/C)$ vs. irradiation time are shown in Figure S4, Supplementary Materials.

It can be observed that in some cases, the relative concentration of diuron decreases under dark conditions, which is due to diuron adsorption on the catalysts surface and depends on the photocatalysts' properties. On one hand diuron molecular size and, on the other hand, the surface area, pore volumes and, especially, pore size distribution of the photocatalysts (pore size in the range 3–18 nm, with average value around 8–9 nm) allow consideration that diffusional problems will not negatively affect the adsorption kinetics [51]. When the light is turned on, diuron concentration decreases much faster because of the photodegradation process. However, adsorption is, probably, also occurring and, therefore, two phenomena can simultaneously occur: diuron adsorption (in darkness and under illumination) and diuron photodegradation (only under illumination). It is also important to mention that as diuron adsorption depends on the sample, the herbicide concentration when the illumination is switched on is not the same in each experiment.

Figure 4a shows that for the TiO_2 (nt) sample the diuron concentration is reduced about 20% due to adsorption in the dark period. Such a reduction is about 10% in the case of TiO_2 (350) and P25, whereas it is almost negligible for TiO_2 samples treated at higher temperatures. Figure 4b shows that diuron adsorption in dark conditions notably increases with the carbon content and in the case of the TiO_2-AC5 (350) and TiO_2-AC10 (350) samples, the adsorption equilibrium is not reached in the 2 h dark period.

The amount of adsorbed diuron is related with the photocatalysts' surface areas. A direct relationship between both parameters has been found for bare TiO_2 and TiO_2-AC samples (Supplementary Materials, Figure S5), being the diuron adsorption capacity of the TiO_2-ACx samples higher than that of bare TiO_2 samples with similar or even larger S_{BET}. It can be pointed out that TiO_2-AC10 (350) adsorbs 90.5% of diuron present in solution

after 2 h in darkness. However, diuron adsorption is similar on P25 and on TiO_2 (350), despite their different S_{BET} values. This highlights that diuron adsorption extent in not only determined by the surface area. Indeed, the crystalline phase composition or the crystallinity degree might play a role.

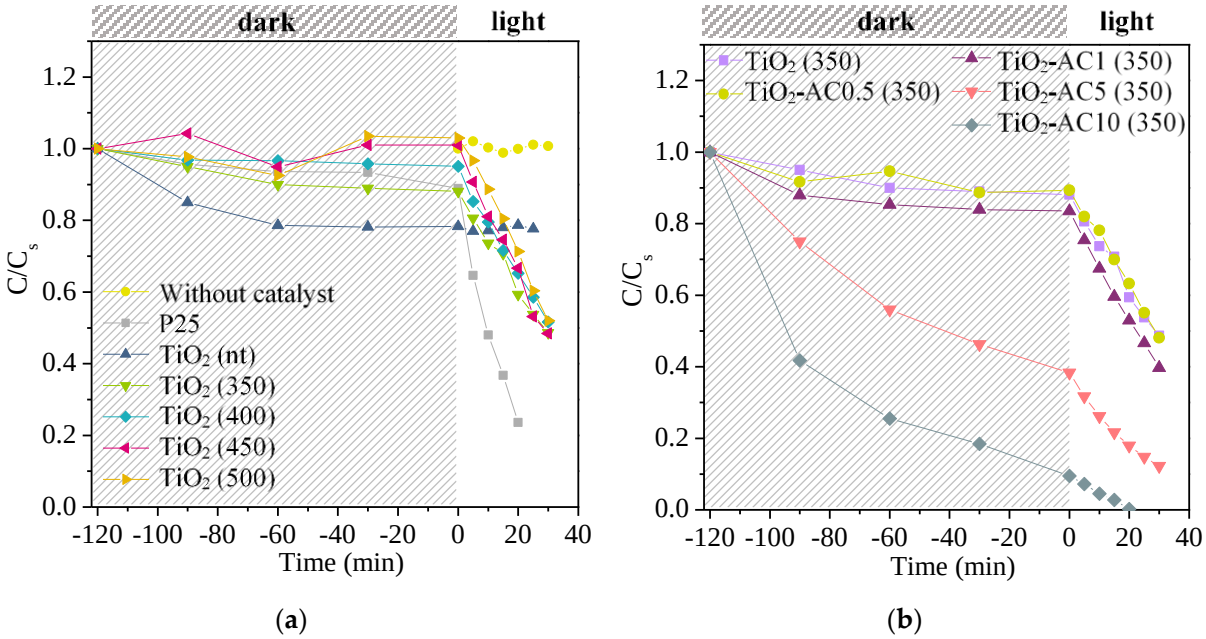

Figure 4. Evolution of the relative concentration of diuron vs. time in the darkness and under illumination using (**a**) P25, TiO_2 (nt) and TiO_2 (T) photocatalysts and (**b**) TiO_2-ACx (350) (x = 0, 0.5, 1, 5, and 10 wt.%) photocatalysts. The first 120 min (negative numbers in *x*-axis), correspond to dark conditions and, from the time identified as 0, the system is irradiated.

Diuron photodegradation does not occur in absence of catalyst (Figure 4a), meaning that diuron photolysis can be neglected in these experimental conditions. The TiO_2 (nt) catalyst has shown to be inactive, while all TiO_2 (T) samples are photoactive leading to similar diuron degradation rates. This means, on one hand, that the post-synthesis heat treatment is necessary to make the samples active and, on the other hand that either the differences between samples are too small to show any effect in the rate of diuron removal, or that there is a compensation of effects, i.e., larger surface area and lower crystallinity is equivalent to lower surface area and higher crystallinity. Many works claim that crystallinity, surface area, and size of TiO_2 particles affect the photocatalytic activity; however it is difficult to estimate the separate contribution of each of them [52,53].

As an example, products of diuron photodegradation obtained when using TiO_2-AC10 (350) were analyzed by ionic chromatography. Short-chain organic acids (1.12 mg/L oxalic acid, 0.24 mg/L acetic acid, 0.06 mg/L formic acid) and chloride ions (0.3 mg/L) were detected in the solution, in agreement with the literature [1,54]. The low concentration of inorganic chloride (product of diuron dechlorination during the early stage of its photocatalytic degradation [55]) suggests that probably most of the chloride species remained adsorbed on the photocatalyst's surface.

Diuron photodegradation over illuminated TiO_2 has been modelled using the Langmuir-Hinshelwood model [56]. For highly diluted solutions, the kinetic model can be simplified to an apparent first-order equation: $Ln(C_0/C) = k_{app} \cdot t$ [57], in which C_0 is the diuron concentration at t = 0, C is the diuron concentration at a certain time t and k_{app} is the apparent rate constant (if photodegradation and adsorption take place simultaneously, k_{app} is an apparent rate constant comprising both phenomena).

Table 2 shows the k_{app} values determined from the plots of Figure S4. It can be observed that k_{app} for P25 is clearly higher than those determined for TiO_2 (T) samples. The higher activity of P25 could be related to its higher degree of crystallinity (87% vs.

76–78% of TiO_2 (T) samples), although TiO_2 (T) samples had smaller mean crystallite size and larger surface area. This underlines the importance of an accurate determination of the crystalline/amorphous proportion of the TiO_2 photocatalysts, and not only of the crystalline phase proportion within the crystalline fraction.

Table 2. Apparent first-order rate constant (k_{app}) for diuron removal with the corresponding linear regression coefficients R^2 and diuron removal efficiency (%) in experiments shown in Figure 4.

Set	Sample	$k_{app} \times 10^3$ (min^{-1})	R^2	Diuron Removal Efficiency * (%)
1	P25	63.4	0.997	76.4
	Without catalyst	0.0	-	0.0
	TiO_2 (nt)	0.0	-	21.4
	TiO_2 (350)	19.2	0.992	40.6
	TiO_2 (400)	19.6	0.998	34.8
	TiO_2 (450)	18.5	0.997	27.4
	TiO_2 (500)	20.5	0.984	28.7
2	TiO_2 (350)	19.2	0.992	40.6
	TiO_2-AC0.5 (350)	18.9	0.988	36.7
	TiO_2-AC1 (350)	23.6	0.998	47.1
	TiO_2-AC5 (350)	38.4	0.998	82.1
	TiO_2-AC10 (350)	78.2	0.994	99.8

* Removal efficiency obtained by adsorption and photocatalytic degradation, after 120 min in darkness and 20 min under irradiation.

Regarding TiO_2-ACx samples, data of Table 2, Set 2, show that k_{app} increases with the carbon content and, consequently, with the adsorption capacity of these photocatalysts. The k_{app} value is highest for TiO_2-AC10 (350), 78.2 $\times$ 10^{-3} min^{-1}, which surpasses the k_{app} value obtained for P25 (63.4 $\times$ 10^{-3} min^{-1}). However, as the k_{app} values have been calculated with different initial diuron concentrations (C_0), it is clear that the comparison between samples is not completely fair. Because of that, the photocatalysts behavior has also been measured in terms of diuron removal efficiency after 120 min in darkness and 20 min under irradiation (at 20 min irradiation time diuron removal is complete in one of the catalysts) and calculated as the decrease percentage of the initial diuron concentration (C_s) (by adsorption and photodegradation). Data are presented in Table 2, where it can be observed that for samples of Set 1, the highest diuron removal is achieved with P25 and TiO_2 (T) samples are more efficient than TiO_2 (nt), being TiO_2 (350) is the one leading to the highest diuron removal, which can be related to its higher surface area. Samples of Set 2 (TiO_2-ACx (350)) catalysts are more efficient for diuron removal than TiO_2 (T) counterparts, which is due to the important diuron adsorption in the carbon-containing hybrid photocatalysts. The percentage of diuron removed from water increases with the carbon content, samples TiO_2-AC5 (350) and TiO_2-AC10 (350) are more efficient than P25 (82.1 and 99.8 vs. 76.4% efficiencies, respectively, after 120 min in darkness and 20 min under irradiation). In the literature, such high photodegradation efficiencies in so short irradiation times have not been reported before for TiO_2-based photocatalysts. Other research groups have studied the photocatalytic behavior of metal-TiO_2 catalysts in diuron photodecomposition. Menzi et al. [58] proved that after 60 min irradiation time, diuron photodegradation was 51% and 75% for pure TiO_2 and for Au-TiO_2, respectively, while it reached 100% for the hybrid Pt-TiO_2 photocatalyst. Foura et al. [59] prepared a W-TiO_2 (3 wt.% W) that exhibited better photoactivity than pure TiO_2 (k_{app} were 43.6 $\times$ 10^3 and 21.9 $\times$ 10^3 min^{-1}, respectively). Cruz et al. [60] studied the photodegradation of diuron using graphene oxide-TiO_2 catalyst and showed that 79 min of irradiation were needed to achieve 50% diuron conversion. Bamba et al. [32] studied TiO_2 photocatalysts containing activated carbon and reported a diuron removal efficiency of 99.95 and 98.61% after 90 min in darkness and 180 min under irradiation for P25 and TiO_2-AC, respectively (TiO_2-AC was prepared by sol-gel method, with a surface area of 206 m^2/g and 99.2 wt.% of anatase).

The apparent first-order rate constant for their TiO_2-AC catalyst (with Ti/C ratio of 2/1) was 26 × 10^{-3} min^{-1}, which is well below the k_{app} values obtained in this investigation.

In our work, photocatalysts with nominal AC loading beyond 10 wt.% were not studied because, on one hand, 10 wt.% AC leads to an important diuron adsorption and it is much more difficult to analyze the photocatalytic process and, on the other hand, a high AC loading could result in an important covering of the TiO_2 surface, limiting it capacity to absorb light.

In the case of the TiO_2-AC10 (350) sample, diuron removal was also evaluated after adsorption periods in darkness of variable duration, ranging from 1 min to 360 min, and keeping the same irradiation time indicated above, 20 min. Figure 5 shows the evolution of the relative diuron concentration, C/C_s, vs. time, and Table 3 compiles the calculated apparent first-order rate constant values. Data of Table 3 show that k_{app} increases with the adsorption time in darkness up to120 min (at this time more than 90% of diuron is adsorbed at the catalyst surface) and then, it decreases for the sample remaining 360 min in darkness.

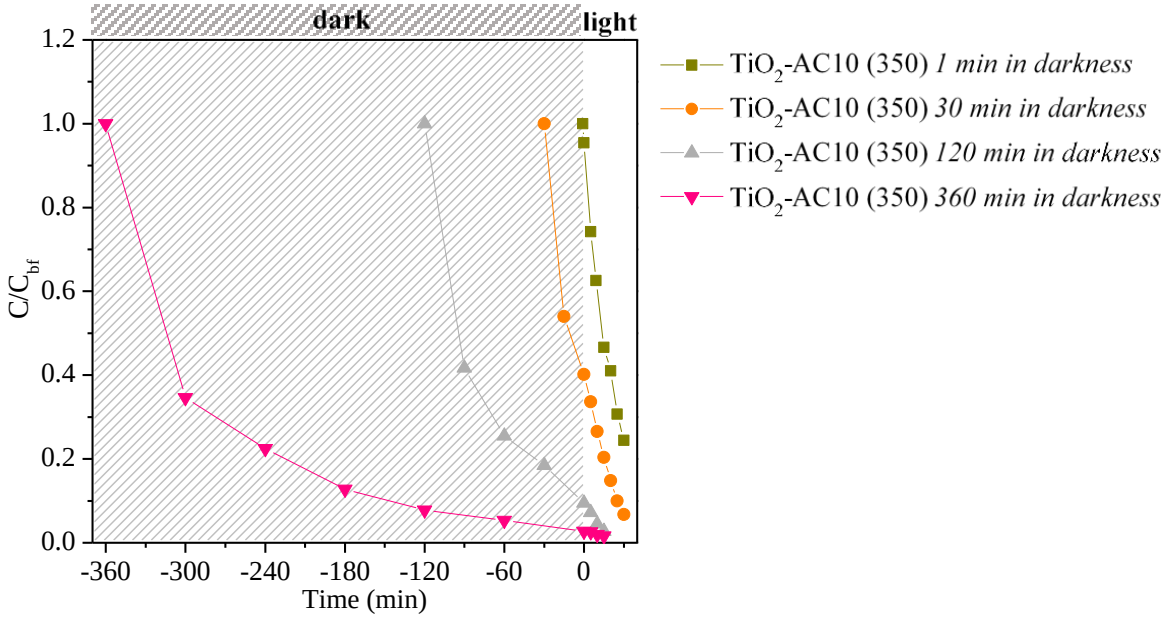

Figure 5. Evolution of the relative diuron concentration with time using TiO_2-AC10 (350) sample in darkness (for 1, 30, 120 or 360 min) and under illumination conditions. The corresponding Ln(C_0/C) vs. irradiation time plots for the removal of diuron under simulated solar light in the case of TiO_2-AC10 (350) sample is reported in Figure S6, in the Supplementary Materials.

Table 3. Apparent first-order rate constant (k_{app}) for TiO_2-AC10 (350) sample in experiments with different pre-adsorption time in darkness and the corresponding linear regression coefficient R^2.

Sample	Time in Darkness (min)	k_{app} × 10^3 (min^{-1})	R^2
TiO_2-AC10 (350)	1	45.2	0.998
TiO_2-AC10 (350)	30	54.3	0.987
TiO_2-AC10 (350)	120	78.2	0.994
TiO_2-AC10 (350)	360	33.6	0.959

Thus, to compare experiments with similar diuron concentration at t = 0 (C_0), the dark period should not be the same. Such a comparison has been done keeping samples TiO_2 (450) and TiO_2 (500) 2 h in darkness prior to illumination and sample TiO_2-AC10 (350) only one minute (Figure S7 (Supplementary Materials)). For TiO_2 (450) and TiO_2 (500) samples, adsorption equilibrium was reached before the light was turned on, meaning that under illumination diuron was removed from solution exclusively by its photocatalytic degrada-

tion. In contrast, in the case of TiO_2-AC10 (350) diuron adsorption and photodegradation simultaneously occurred under irradiation. Comparison of the calculated k_{app} for these experiments (18.5×10^{-3}, 20.5×10^{-3}, 45.2×10^{-3} min^{-1} for TiO_2 (450), TiO_2 (500) and TiO_2-AC10 (350), respectively) shows that the k_{app} for TiO_2-AC10 (350) is clearly higher and, considering that k_{app} for most of the bare or low-carbon TiO_2 samples is around 20×10^{-3}, it can be estimated that the contribution of adsorption to the combined process is more that 50%.

Comparing all the tested samples, it can be concluded that the selection of an optimum material would depend on the operational procedure. If the system continuously operates under Ultraviolet A (UV-A) light irradiation, P25 would be the most efficient material. By contrast, if the operational procedure includes a period of time in darkness, in which adsorption can occur independently of degradation, TiO_2-ACx (350) samples, particularly TiO_2-AC10 (350), would be more effective for diuron removal.

Another point to highlight is that TiO_2-AC samples can be considered quite robust, since the samples remain undamaged after the different processes in which they are used.

2.6. Total Organic Carbon (TOC) Measurements

Considering the relevance and extent of diuron adsorption on TiO_2-ACx (350) hybrid photocatalysts, additional experiments were conducted to study the potential desorption of adsorbed diuron (or other intermediates of diuron degradation) and their subsequent photooxidation. Samples TiO_2-AC1 (350) and TiO_2-AC10 (350) were treated as follows: they were put in contact with 100 mL of aqueous solution of diuron (10 mg/L), maintained for 2 h in darkness and then, irradiated for 1 h. In these conditions the complete removal of diuron from solution occurred with both samples (see Supplementary Materials, Figure S8). Afterwards, the solids were recovered by filtration and mixed with 100 mL ultrapure water under stirring. The suspension was further irradiated, and the total organic carbon (TOC) in the solution was periodically measured (Supplementary Materials, Figure S9). For both samples, an increase of the TOC value was observed, in the first 30 min in the case of TiO_2-AC1 (350) and in a period of about 180 min in the case of TiO_2-AC10 (350), followed by a subsequent decrease. This reveals that diuron, or other partially oxidized organic intermediate compounds, desorb from the catalysts, and are further photocatalytically degraded. As expected, the number of desorbed species is larger for TiO_2-AC10 (350) than for TiO_2-AC1 (350). These results indicate that illumination could be used to regenerate TiO_2-carbon hybrid photocatalysts and so, they could be used again. Additional tests would be needed to state up to which extent the photocatalytic activity is kept after several regeneration cycles.

3. Materials and Methods

3.1. Preparation of TiO_2 and TiO_2-AC Photocatalysts

TiO_2 and TiO_2-AC photocatalysts were prepared by sol-gel as follows [61]: 9.3 mL titanium tetraisopropoxide (TTIP) (97%, Sigma-Aldrich, St. Louis, MO, USA) were mixed with 17.5 mL glacial acetic acid (HAc) (99%, Sigma-Aldrich) at 0 °C. Then, to prepare TiO_2 materials, 197.5 mL distilled water were added dropwise under vigorous stirring. To obtain hybrid TiO_2-AC photocatalysts, a certain amount of activated carbon (see next section) (0.01, 0.02, 0.13 or 0.27 g, to obtain catalysts with nominal 0.5, 1, 5, and 10 wt.% AC, respectively) was added to 5 mL water, and this mixture was incorporated dropwise to the TTIP/HAc solution; then, water was added dropwise up to a total volume of 197.5 mL. Afterwards, in both preparations the mixture was ultrasonicated for 30 min, stirred for 5 h and the formed suspension was aged in an oven at 70 °C for 12 h. The solid product was dried at 100 °C for 12 h and crushed into a fine powder. Then, the obtained TiO_2 was heat-treated in air at 350, 400, 450 or 500 °C for 2 h (muffle, 5 °C/min) to increase the crystallinity and to remove carbon residues from the synthesis process. The nomenclature used is TiO_2 (T), where T is the temperature of the heat treatment. A non-treated sample named TiO_2 (nt), where nt means not treated, was also studied. The TiO_2-AC catalysts

were submitted to a post-synthesis heat treatment in air at 350 °C for 2 h (muffle, 5 °C/min). This temperature has been chosen because it allows the obtaining of a good compromise between the crystallinity of the TiO_2-AC materials and their carbon content remaining after treatment. The samples were named TiO_2-ACx (350), where x refers to the nominal AC wt.% indicated above. Degussa Aeroxide P25 TiO_2 has been used as a reference material.

3.2. Preparation of Activated Carbon

The activated carbon (AC) was prepared by hydrothermal carbonization of saccharose (99.5%, Sigma-Aldrich) as follows [62]: 12 g saccharose were mixed with 21 mL water (1.6 M solution). Then, the mixture was transferred to a 50 mL Teflon-lined stainless-steel autoclave and heated in an oven at 180 °C for 12 h. After cooling down to room temperature, the solid product was recovered by filtration, washed with distilled water and dried (110 °C, 5 h). Finally, it was activated with CO_2 (80 mL/min) at 800 °C (5 °C/min heating rate) for 5 h.

3.3. Photocatalysts' Characterization

Porosity and specific surface area of the prepared photocatalysts were characterized by N_2 adsorption-desorption at −196 °C (after outgassing at 250 °C, 4 h) in a Quantachrome Autosorb-6B equipment (Quantachrome Instruments, Boynton Beach, FL, USA). The specific BET surface area (S_{BET}) and the micropore volume (V_{N2}) were determined by applying the Brunauer–Emmett–Teller (BET) and the Dubinin–Radushkevich equations to the N_2 adsorption isotherms, respectively. The mesopore volume (V_{meso}) was estimated by the difference of the volume of N_2 adsorbed as liquid at $P/P_0 = 0.9$ and $P/P_0 = 0.2$, while the total pore volume (V_T) was determined as the volume of N_2 adsorbed at $P/P_0 = 0.99$ [63–65]. The pore size distribution was calculated using the adsorption branch from the N_2 isotherm, by using BJH (Barrett-Joyner- Halenda) method.

XRD analysis was performed in a SEIFERT 2002 equipment (Rich. Seifert & Co., Ahrensburg, Germany), using Cu Kα (1.54 Å) radiation, in the 6–80° 2θ range, with a scanning velocity of 2°/min. The average crystallite size, referred to as crystal size, was calculated by Scherrer's equation (Equation (1)) [66]:

$$B = \frac{K\lambda}{\beta \cos\theta} \quad (1)$$

where B is the average crystallite size (nm); K is a constant with a value of 0.9 [67]; λ is the wavelength of the radiation source; β is the full width at half maximum intensity (FWHM) and θ is the angle associated with the main peak corresponding to the studied phase (2θ values of 25.3° and 27.5° for anatase (A) and rutile (R), respectively). The amount of anatase and rutile and the percentage of amorphous TiO_2 have been calculated as explained in a previous work [23].

The actual carbon content of the TiO_2-ACx (350) samples was determined by thermogravimetry (TA Instruments, New Castle, DE, USA) (TG SDT Q600, air flow (50 mL/min), 10 °C/min up to 900 °C).

Scanning Electron Microscopy (SEM, JSM-840 microscope (JEOL, Tokyo, Japan) with scintillator-photomultiplier type secondary electron detector) was used to analyze the morphology of the obtained AC and TiO_2-ACx (nt) samples.

3.4. Photocatalytic Activity Measurements

The experiments were carried out, under stirring, inside a Suntest XLS+ reaction chamber (Atlas Material Testing Technology BV, Gelnhausen, Germany) equipped with a 1700 W Xenon arc lamp and a Solar ID65 filter to limit the UV radiation at 320 nm for simulating solar exposition, according to ICH Q1B guidelines. The spectral distribution is reported in Figure S10 in Supplementary Materials.

A batch beaker-type glass reactor was used at atmospheric pressure. In each experiment, 100 mg of photocatalyst were dispersed under stirring in 100 mL of a 10 mg/L

aqueous solution of diuron ($C_9H_{10}Cl_2N_2O$, 98%, Sigma-Aldrich). The suspension was exposed to simulated solar light at 250 Wm^{-2}, which corresponds to an average solar radiation in a summer day in southern Europe [68]. The distance between the light source and the reactor was 32 cm. All the tests were performed using 1 g/L photocatalyst concentration since it has been shown to be the optimum one for P25 [69].

Prior to irradiation, the catalyst suspension was stirred for 2 h in darkness to ensure the adsorption/desorption equilibrium (unless a different specific protocol was mentioned). 1 mL solution was periodically sampled, filtered (0.20 μm filter (Chromafil®PET-20/25)), and analyzed by UV-Vis spectrophotometry (CARY 100 Scan UV-visible spectrophotometer) (Agilent Technologies, Santa Clara, CA, USA). The process was followed by monitoring the intensity of the main absorption peak, at λ = 248 nm. Total organic carbon (TOC) was measured using a Shimadzu TOC-L analyzer. In some cases, solutions were also analyzed by ionic chromatography (Metrohm 790 IC) using a conductivity detector.

4. Conclusions

TiO_2 and TiO_2-carbon photocatalysts have been synthetized by sol-gel, being the first submitted to a post-synthesis heat treatment at different temperatures, and the second prepared with different amounts of activated carbon (AC) and heat-treated at 350 °C.

The bare TiO_2 samples contain only anatase (about 62–78%) and, as the temperature of the heat treatment increases, the surface area decreases and the anatase crystallite size increases, being the anatase content for samples treated between 350 and 500 °C essentially constant. The surface area of the TiO_2-carbon samples increases with the carbon content, and the incorporation of AC does not affect TiO_2 crystallinity.

Diuron adsorption plays an important role in the photocatalysts behavior. Results obtained with bare TiO_2 samples reveal that diuron adsorption extent in not only determined by the surface area. In contrast, a clear relationship between surface area and diuron adsorption has been observed in TiO_2-ACx (350) catalysts. P25 shows the highest photocatalytic activity for diuron degradation, which can be explained by its higher crystallinity. However, the largest diuron removal, 99.8%, was achieved with the TiO_2 sample prepared with 10 wt.% AC. It is due to the combination of adsorption and photodegradation, being this an interesting result in comparison with those previously published in the literature, especially for the low illumination time used.

Our results highlight that for this application, the selection of an optimum material would depend on the operational procedure: P25 shows the best performance in illumination conditions, but carbon-containing hybrid samples are very efficient if the process includes dark periods in which adsorption takes place, even more considering that adsorbed diuron can be desorbed afterwards and further oxidized. This points out to potential regeneration procedure that merits further research.

Supplementary Materials: The following are available online at https://www.mdpi.com/article/10.3390/catal11040457/s1, Figure S1: (a) TG and (b) DTG curves for TiO_2 (350) and the TiO_2-ACx (350) samples.; Figure S2: Pore size distribution determined from the nitrogen adsorption isotherms by means of the BJH method.; Table S1: Weight loss (wt.%) in the four temperature intervals observed in the TG-DTG profiles (Figure S2) and calculated carbon content.; Table S2: Textural properties for P25, TiO_2 (nt) and TiO_2 (T) samples (Set 1) and for AC, TiO_2 (350) and TiO_2-ACx (350) samples (Set 2).; Figure S3: XRD pattern for AC; Figure S4: $Ln(C_0/C)$ vs. irradiation time for: (a) P25, TiO_2 (nt) and TiO_2 (T) photocatalysts and (b) TiO_2-ACx (350) (x = 0, 0.5, 1, 5, and 10 wt.%) hybrid photocatalysts. Reaction: degradation of diuron under simulated solar light.; Figure S5: Diuron adsorption (as % respect to the initial diuron concentration) after 2 h in dark and S_{BET} values for: (a) P25, TiO_2 (nt) and TiO_2 (T) photocatalysts and (b) TiO_2-ACx (350) (x = 0, 0.5, 1, 5, and 10 wt.%).; Figure S6: $Ln(C_0/C)$ vs. irradiation time for TiO_2-AC10 (350) sample after 1, 30, 120, or 360 min in dark conditions. Reaction: diuron degradation under simulated solar light.; Figure S7: Evolution of the relative diuron concentration vs. time in dark and under illumination conditions for TiO_2-AC10 (350) sample (1 min in darkness) and for TiO_2 (450) and TiO_2 (500) samples (2 h in darkness).; Figure S8: Relative diuron concentration vs. time in darkness (2 h) and under illumination conditions (1 h) for

TiO_2-AC1 (350) and TiO_2-AC10 (350) samples (after 1 h irradiation the complete removal of diuron was observed).; Figure S9: TOC values vs. irradiation time determined during reuse of TiO_2-AC1 (350) and TiO_2-AC10 (350) hybrid photocatalysts. Reaction: diuron degradation under simulated solar light.; Figure S10: Spectral distribution of the simulated solar light. Measurements have been performed using a wideband RPS900-W rapid portable spectroradiometer from International Light Technology.

Author Contributions: Conceptualization, M.Á.L.-R., M.d.C.R.-M. and N.K.; methodology, A.A.-P., M.Á.L.-R., M.d.C.R.-M. and N.K.; investigation, A.A.-P., M.Á.L.-R., M.d.C.R.-M., P.G.-M. and N.K.; resources, M.Á.L.-R. and M.d.C.R.-M.; data curation, A.A.-P., M.Á.L.-R., M.d.C.R.-M. and N.K.; writing—original draft preparation, A.A.-P., M.Á.L.-R. and M.d.C.R.-M.; writing—review and editing, A.A.-P., M.Á.L.-R., M.d.C.R.-M. and N.K.; supervision, M.Á.L.-R., M.d.C.R.-M. and N.K.; project administration, M.Á.L.-R., M.d.C.R.-M. and N.K.; funding acquisition, M.Á.L.-R. and M.d.C.R.-M. All authors have read and agreed to the published version of the manuscript.

Funding: This research was funded by the Spanish Ministry of Science, Innovation and Universities, MICIU, and Fondo Europeo de Desarrollo Regional, FEDER, (RTI2018-095291-B-I00), by Generalitat Valenciana and FEDER (GV/FEDER (PROMETEO/2018/076)) and by the University of Alicante (VIGROB-136).

Acknowledgments: The authors thank funding to MICIU/FEDER, project of reference RTI2018-095291-B-I00, to GV/FEDER (PROMETEO/2018/076) and to University of Alicante (VIGROB-136).

Conflicts of Interest: The authors declare no conflict of interest.

References

1. Solís, R.R.; Rivas, F.J.; Martínez-Piernas, A.; Agüera, A. Ozonation, photocatalysis and photocatalytic ozonation of diuron: Intermediates identification. *Chem. Eng. J.* **2016**, *292*, 72–81. [CrossRef]
2. Gavrilescu, M. Fate of pesticides in the environment. *Eng. Life Sci.* **2005**, *5*, 497–526. [CrossRef]
3. Wessels, J.S.; Van der Veen, R. The action of some derivatives of phenylurethan and of 3-phenyl-1, 1-dimethylurea on the Hill reaction. *Biochim. Biophys. Acta* **1956**, *19*, 548–549. [CrossRef]
4. Giacomazzi, S.; Cochet, N. Environmental impact of diuron transformation: A review. *Chemosphere* **2004**, *56*, 1021–1032. [CrossRef]
5. Wauchope, R.D. The pesticide content of surface water draining from agricultural field. *J. Environ. Qual.* **1978**, *7*, 459–472. [CrossRef]
6. Thurman, E.M.; Bastian, K.C.; Mollhagen, T. Occurrence of cotton herbicides and insecticides in playa lakes of the high Plains of West Texas. *Sci. Total Environ.* **2000**, *248*, 189–200. [CrossRef]
7. University of Hertfordshire (UK) Pesticide Properties Database. Available online: http://sitem.herts.ac.uk/aeru/ppdb/en/Reports/260.htm (accessed on 24 February 2021).
8. Loos, R.; Gawlik, B.M.; Locoro, G.; Rimaviciute, E.; Contini, S.; Bidoglio, G. EU-wide survey of polar organic persistent pollutants in European river waters. *Environ. Pollut.* **2009**, *157*, 561–568. [CrossRef] [PubMed]
9. European Commission. EU Directive 2013/39/EU of the European Parliament and The Council of 12 August 2013, Amending Directives 2000/60/EC and 2008/105/EC as regards priority substances in the field of water policy. *Off. J. Eur. Union* **2013**, *226*, 1–17.
10. Bamba, D.; Atheba, P.; Robert, D.; Trokourey, A.; Dongui, B. Photocatalytic degradation of the diuron pesticide. *Environ. Chem. Lett.* **2008**, *6*, 163–167. [CrossRef]
11. El Madani, M.; Guillard, C.; Pérol, N.; Chovelon, J.M.; El Azzouzi, M.; Zrineh, A.; Herrmann, J.M. Photocatalytic degradation of diuron in aqueous solution in presence of two industrial titania catalysts, either as suspended powders or deposited on flexible industrial photoresistant papers. *Appl. Catal. B Environ.* **2006**, *65*, 70–76. [CrossRef]
12. Prieto-Rodriguez, L.; Miralles-Cuevas, S.; Oller, I.; Agüera, A.; Puma, G.L.; Malato, S. Treatment of emerging contaminants in wastewater treatment plants (WWTP) effluents by solar photocatalysis using low TiO 2 concentrations. *J. Hazard. Mater.* **2012**, *211–212*, 131–137. [CrossRef]
13. Ribeiro, A.R.; Nunes, O.C.; Pereira, M.F.R.; Silva, A.M.T. An overview on the advanced oxidation processes applied for the treatment of water pollutants defined in the recently launched Directive 2013/39/EU. *Environ. Int.* **2015**, *75*, 33–51. [CrossRef] [PubMed]
14. Malato, S.; Blanco, J.; Vidal, A.; Alarcón, D.; Maldonado, M.I.; Cáceres, J.; Gernjak, W. Applied studies in solar photocatalytic detoxification: An overview. *Sol. Energy* **2003**, *75*, 329–336. [CrossRef]
15. Foo, C.; Li, Y.; Lebedev, K.; Chen, T.; Day, S.; Tang, C.; Tsang, S.C.E. Characterisation of oxygen defects and nitrogen impurities in TiO_2 photocatalysts using variable-temperature X-ray powder diffraction. *Nat. Commun.* **2021**, *12*, 1–14. [CrossRef]
16. Guo, Q.; Zhou, C.; Ma, Z.; Yang, X. Fundamentals of TiO_2 Photocatalysis: Concepts, Mechanisms, and Challenges. *Adv. Mater.* **2019**, *31*, 1–26. [CrossRef]

17. Nakata, K.; Fujishima, A. TiO_2 photocatalysis: Design and applications. *J. Photochem. Photobiol. C Photochem. Rev.* **2012**, *13*, 169–189. [CrossRef]
18. Malato, S.; Cáceres, J.; Fernández-Alba, A.R.; Piedra, L.; Hernando, M.D.; Agüera, A.; Vial, I. Photocatalytic treatment of diuron by solar photocatalysis: Evaluation of main intermediates and toxicity. *Environ. Sci. Technol.* **2003**, *37*, 2516–2524. [CrossRef] [PubMed]
19. Hincapié, M.; Maldonado, M.I.; Oller, I.; Gernjak, W.; Sánchez-Pérez, J.A.; Ballesteros, M.M.; Malato, S. Solar photocatalytic degradation and detoxification of EU priority substances. *Catal. Today* **2005**, *101*, 203–210. [CrossRef]
20. Yaemsunthorn, K.; Kobielusz, M.; Macyk, W. TiO_2 with Tunable Anatase-to-Rutile Nanoparticles Ratios: How Does the Photoactivity Depend on the Phase Composition and the Nature of Photocatalytic Reaction? *ACS Appl. Nano Mater.* **2021**, *4*, 633–643. [CrossRef]
21. Telegang Chekem, C.; Goetz, V.; Richardson, Y.; Plantard, G.; Blin, J. Modelling of adsorption/photodegradation phenomena on AC-TiO_2 composite catalysts for water treatment detoxification. *Catal. Today* **2019**, *328*, 183–188. [CrossRef]
22. Ghosh, M.; Lohrasbi, M.; Chuang, S.S.C.; Jana, S.C. Mesoporous Titanium Dioxide Nanofibers with a Significantly Enhanced Photocatalytic Activity. *ChemCatChem* **2016**, *8*, 2525–2535. [CrossRef]
23. Amorós-Pérez, A.; Cano-Casanova, L.; Castillo-Deltell, A.; Román-Martínez, M.C.; Lillo-Ródenas, M.Á. TiO_2 Modification with Transition Metallic Species (Cr, Co, Ni and Cu) for Photocatalytic Abatement of Acetic Acid in Liquid Phase and Propene in Gas Phase. *Materials* **2019**, *12*, 40. [CrossRef]
24. Ghosh, M.; Liu, J.; Chuang, S.S.C.; Jana, S.C. Fabrication of Hierarchical V_2O_5 Nanorods on TiO_2 Nanofibers and Their Enhanced Photocatalytic Activity under Visible Light. *ChemCatChem* **2018**, *10*, 3305–3318. [CrossRef]
25. Yang, Z.; Yin, L.; Ou, E.; Wang, Y.; Peng, L.; Wang, J. Transition metal doped mesoporous titania with a crystalline framework as catalysts for oxidation of p-bromotoluene to p -bromobenzaldehyde. *Front. Chem. Eng. China* **2008**, *2*, 296–300. [CrossRef]
26. Suzuki, N.; Okazaki, A.; Kuriyama, H.; Serizawa, I.; Hara, A.; Hirano, Y.; Nakabayashi, Y.; Roy, N.; Terashima, C.; Nakata, K.; et al. Synthesis of mesoporous TiO2/boron-doped diamond photocatalyst and its photocatalytic activity under deep UV light (λ = 222 nm) irradiation. *Molecules* **2018**, *23*, 3095. [CrossRef]
27. Hao, R.; Wang, G.; Jiang, C.; Tang, H.; Xu, Q. In situ hydrothermal synthesis of g-C_3N_4/TiO_2 heterojunction photocatalysts with high specific surface area for Rhodamine B degradation. *Appl. Surf. Sci.* **2017**, *411*, 400–410. [CrossRef]
28. Leary, R.; Westwood, A. Carbonaceous nanomaterials for the enhancement of TiO2 photocatalysis. *Carbon N. Y.* **2011**, *49*, 741–772. [CrossRef]
29. Zeng, G.; You, H.; Du, M.; Zhang, Y.; Ding, Y.; Xu, C.; Liu, B.; Chen, B.; Pan, X. Enhancement of photocatalytic activity of TiO_2 by immobilization on activated carbon for degradation of aquatic naphthalene under sunlight irradiation. *Chem. Eng. J.* **2021**, *412*, 128498. [CrossRef]
30. Areerachakul, N.; Vigneswaran, S.; Ngo, H.H.; Kandasamy, J. Granular activated carbon (GAC) adsorption-photocatalysis hybrid system in the removal of herbicide from water. *Sep. Purif. Technol.* **2007**, *55*, 206–211. [CrossRef]
31. Kim, S.H.; Ngo, H.H.; Shon, H.K.; Vigneswaran, S. Adsorption and photocatalysis kinetics of herbicide onto titanium oxide and powdered activated carbon. *Sep. Purif. Technol.* **2008**, *58*, 335–342. [CrossRef]
32. Bamba, D.; Coulibaly, M.; Fort, C.I.; Coteț, C.L.; Pap, Z.; Vajda, K.; Zoro, E.G.; Yao, N.A.; Danciu, V.; Robert, D. Synthesis and characterization of TiO2/C nanomaterials: Applications in water treatment. *Phys. Status Solidi Basic Res.* **2015**, *252*, 2503–2511. [CrossRef]
33. Anirudhan, T.S.; Shainy, F.; Manasa Mohan, A. Fabrication of zinc oxide nanorod incorporated carboxylic graphene/polyaniline composite and its photocatalytic activity for the effective degradation of diuron from aqueous solutions. *Sol. Energy* **2018**, *171*, 534–546. [CrossRef]
34. Anirudhan, T.S.; Christa, J.; Shainy, F. Magnetic titanium dioxide embedded molecularly imprinted polymer nanocomposite for the degradation of diuron under visible light. *React. Funct. Polym.* **2020**, *152*, 104597. [CrossRef]
35. Toyoda, M.; Nanbu, Y.; Nakazawa, Y.; Hirano, M.; Inagaki, M. Effect of crystallinity of anatase on photoactivity for methyleneblue decomposition in water. *Appl. Catal. B Environ.* **2004**, *49*, 227–232. [CrossRef]
36. Inagaki, M.; Nonaka, R.; Tryba, B.; Morawski, A.W. Dependence of photocatalytic activity of anatase powders on their crystallinity. *Chemosphere* **2006**, *64*, 437–445. [CrossRef] [PubMed]
37. Mozia, S. Effect of calcination temperature on photocatalytic activity of TiO_2. Pahotodecomposition of mono- and polyazo dyes in water. *Pol. J. Chem. Technol.* **2008**, *10*, 42–49. [CrossRef]
38. Cenovar, A.; Paunovic, P.; Grozdanov, A.; Makreski, P.; Fidancevska, E. Preparation of Nano-Crystalline TiO_2 by Sol-Gel Method using Titanium Tetraisopropoxide (TTIP) as a Precursor. *Adv. Nat. Sci. Theory Appl.* **2012**, *1*, 133–142.
39. Sayilkan, F.; Asiltürk, M.; Sayilkan, H.; Önal, Y.; Akarsu, M.; Arpaç, E. Characterization of TiO_2 Synthesized in Alcohol by a Sol-Gel Process: The Effects of Annealing. *Turk. J. Chem.* **2005**, *29*, 697–706.
40. Belhachemi, M.; Khiari, B.; Jeguirim, M.; Sepúlveda-Escribano, A. Characterization of biomass-derived chars. In *Char and Carbon Materials Derived from Biomass*; Elsevier Inc.: Amsterdam, The Netherlands, 2019; pp. 69–108. ISBN 9780128148938.
41. Kusiak-Nejman, E.; Wróbel, R.J.; Kapica-Kozar, J.; Wanag, A.; Szymańska, K.; Mijowska, E.; Morawski, A.W. Hybrid carbon-TiO2 spheres: Investigation of structure, morphology and spectroscopic studies. *Appl. Surf. Sci.* **2018**, *469*, 684–690. [CrossRef]
42. Hung, W.C.; Fu, S.H.; Tseng, J.J.; Chu, H.; Ko, T.H. Study on photocatalytic degradation of gaseous dichloromethane using pure and iron ion-doped TiO2 prepared by the sol-gel method. *Chemosphere* **2007**, *66*, 2142–2151. [CrossRef]

43. Sing, K.S.W.; Everett, D.H.; Haul, R.A.W.; Moscou, L.; Pierotti, R.A.; Rouquerol, J.; Siemieniewska, T. Reporting physisorption data for gas/solid systems with special reference to the determination of surface area and porosity. *Pure Appl. Chem.* **1985**, *57*, 603–619. [CrossRef]
44. Thommes, M.; Kaneko, K.; Neimark, A.V.; Olivier, J.P.; Rodriguez-Reinoso, F.; Rouquerol, J.; Sing, K.S.W. Physisorption of gases, with special reference to the evaluation of surface area and pore size distribution (IUPAC Technical Report). *Pure Appl. Chem.* **2015**, *87*, 1051–1069. [CrossRef]
45. Zhang, K.; Zhou, W.; Zhang, X.; Qu, Y.; Wang, L.; Hu, W.; Pan, K.; Li, M.; Xie, Y.; Jiang, B.; et al. Large-scale synthesis of stable mesoporous black TiO2 nanosheets for efficient solar-driven photocatalytic hydrogen evolution: Via an earth-abundant low-cost biotemplate. *RSC Adv.* **2016**, *6*, 50506–50512. [CrossRef]
46. Fernández-Catalá, J.; Cano-Casanova, L.; Lillo-Ródenas, M.Á.; Berenguer-Murcia, Á.; Cazorla-Amorós, D. Synthesis of TiO_2 with hierarchical porosity for the photooxidation of propene. *Molecules* **2017**, *22*, 2243. [CrossRef] [PubMed]
47. Ouzzine, M.; Lillo-Ródenas, M.A.; Linares-Solano, A. Photocatalytic oxidation of propene in gas phase at low concentration by optimized TiO2 nanoparticles. *Appl. Catal. B Environ.* **2013**, *134–135*, 333–343. [CrossRef]
48. Aguilar, T.; Navas, J.; Alcántara, R.; Fernández-Lorenzo, C.; Gallardo, J.J.; Blanco, G.; Martín-Calleja, J. A route for the synthesis of Cu-doped TiO2 nanoparticles with a very low band gap. *Chem. Phys. Lett.* **2013**, *571*, 49–53. [CrossRef]
49. Shul'ga, Y.M.; Matyushenko, D.V.; Kabachkov, E.N.; Kolesnikova, A.M.; Kurkin, E.N.; Domashnev, I.a.; Brichkin, S.B. Correlation between the E g (1) oscillation frequency and half-width of the (101) peak in the X-ray diffraction pattern of TiO2 anatase nanoparticles. *Tech. Phys.* **2010**, *55*, 141–143. [CrossRef]
50. Jensen, H.; Joensen, K.D.; Jørgensen, J.E.; Pedersen, J.S.; Søgaard, E.G. Characterization of nanosized partly crystalline photocatalysts. *J. Nanopart. Res.* **2004**, *6*, 519–526. [CrossRef]
51. Fontecha-Cámara, M.Á.; López-Ramón, M.V.; Álvarez-Merino, M.A.; Moreno-Castilla, C. Temperature dependence of herbicide adsorption from aqueous solutions on activated carbon fiber and cloth. *Langmuir* **2006**, *22*, 9586–9590. [CrossRef]
52. Fernandes Machado, N.R.C.; Santana, V.S. Influence of thermal treatment on the structure and photocatalytic activity of TiO2 P25. *Catal. Today* **2005**, *107–108*, 595–601. [CrossRef]
53. Ohno, T.; Tokieda, K.; Higashida, S.; Matsumura, M. Synergism between rutile and anatase TiO2 particles in photocatalytic oxidation of naphthalene. *Appl. Catal. A Gen.* **2003**, *244*, 383–391. [CrossRef]
54. Katsumata, H.; Sada, M.; Nakaoka, Y.; Kaneco, S.; Suzuki, T.; Ohta, K. Photocatalytic degradation of diuron in aqueous solution by platinized TiO2. *J. Hazard. Mater.* **2009**, *171*, 1081–1087. [CrossRef] [PubMed]
55. Kouamé, A.N.; Masson, R.; Robert, D.; Keller, N.; Keller, V. β-SiC foams as a promising structured photocatalytic support for water and air detoxification. *Catal. Today* **2013**, *209*, 13–20. [CrossRef]
56. Kouamé, N.A.; Robert, D.; Keller, V.; Keller, N.; Pham, C.; Nguyen, P. Preliminary study of the use of β-SiC foam as a photocatalytic support for water treatment. *Catal. Today* **2011**, *161*, 3–7. [CrossRef]
57. Bamba, D.; Coulibaly, M.; Robert, D. Nitrogen-containing organic compounds: Origins, toxicity and conditions of their photocatalytic mineralization over TiO2. *Sci. Total Environ.* **2017**, *580*, 1489–1504. [CrossRef]
58. Mezni, A.; Saber, N.B.; Bukhari, A.; Ibrahim, M.M.; Al-Talhi, H.; Alshehri, N.A.; Wazir, S.A.; El-Sheshtawy, H.S.; Altalhi, T. Plasmonic hybrid platinum-titania nanocomposites as highly active photocatalysts: Self-cleaning of cotton fiber under solar light. *J. Mater. Res. Technol.* **2020**, *9*, 1447–1456. [CrossRef]
59. Foura, G.; Soualah, A.; Robert, D. Effect of W doping level on TiO_2 on the photocatalytic degradation of Diuron. *Water Sci. Technol.* **2017**, *75*, 20–27. [CrossRef]
60. Cruz, M.; Gomez, C.; Duran-Valle, C.J.; Pastrana-Martínez, L.M.; Faria, J.L.; Silva, A.M.T.; Faraldos, M.; Bahamonde, A. Bare TiO2 and graphene oxide TiO_2 photocatalysts on the degradation of selected pesticides and influence of the water matrix. *Appl. Surf. Sci.* **2017**, *416*, 1013–1021. [CrossRef]
61. Amorós-Pérez, A.; Cano-Casanova, L.; Lillo-Ródenas, M.Á.; Román-Martínez, M.C. Cu/TiO_2 photocatalysts for the conversion of acetic acid into biogas and hydrogen. *Catal. Today* **2017**, *287*, 78–84. [CrossRef]
62. Romero-Anaya, A.J.; Ouzzine, M.; Lillo-Ródenas, M.A.; Linares-Solano, A. Spherical carbons: Synthesis, characterization and activation processes. *Carbon N. Y.* **2014**, *68*, 296–307. [CrossRef]
63. Brunauer, S.; Emmett, P.H.; Teller, E. Adsorption of Gases in Multimolecular Layers. *J. Am. Chem. Soc.* **1938**, *60*, 309–319. [CrossRef]
64. Rodriguez-Reinoso, F.; Linares-Solano, A. *Microporous Structure of Activated Carbons as Revealed by Adsorption Methods*; Thrower, P.A., Ed.; Marcel Dekker: New York, NY, USA, 1989; Volume 21, ISBN 0-8247-7939-8.
65. Joyner, L.G.; Barrett, E.P.; Skold, R. The Determination of Pore Volume and Area Distributions in Porous Substances. II. Comparison between Nitrogen Isotherm and Mercury Porosimeter Methods. *J. Am. Ceram. Soc.* **1951**, *73*, 3155–3158. [CrossRef]
66. Jenkins, R.; Snyder, R.L. *Introduction to X-Ray Powder Diffractometry*; John Wiley and Sons: New York, NY, USA, 1996; ISBN 978-0-471-51339-1.
67. Praveen, P.; Viruthagiri, G.; Mugundan, S.; Shanmugam, N. Structural, optical and morphological analyses of pristine titanium di-oxide nanoparticles–synthesized via sol-gel route. *Spectrochim. Acta A Mol. Biomol. Spectrosc.* **2014**, *117*, 622–629. [CrossRef] [PubMed]

68. Global Solar Atlas. Available online: https://globalsolaratlas.info/map (accessed on 25 March 2020).
69. Garcia-Muñoz, P.; Dachtler, W.; Altmayer, B.; Schulz, R.; Robert, D.; Seitz, F.; Rosenfeldt, R.; Keller, N. Reaction pathways, kinetics and toxicity assessment during the photocatalytic degradation of glyphosate and myclobutanil pesticides: Influence of the aqueous matrix. *Chem. Eng. J.* **2020**, *384*, 123315. [CrossRef]